Viscous boundary layer effects on the Myers impedance boundary condition

Edward J. Brambley[*]

University of Cambridge, UK

This paper considers the effects of a thin laminar compressible viscous boundary layer over acoustic linings.

The presence of a vanishingly-thin nonviscous boundary layer at a fluid–solid interface is know to lead to the so-called Myers boundary condition of continuity of normal particle displacement. This boundary condition is now known to lead to instability when applied to an acoustically-lined duct with flow. Despite this, due to a lack of an alternative, the Myers boundary condition is still widely used, with any instability artifacts being removed by artificial smoothing.

In the last couple of years, efforts have been made to resolve these issues by modelling a sheared mean flow, using the Pridmore-Brown equation. By satisfying the no-slip boundary condition at the wall, the hydrodynamic instability is removed. However, introducing a smoothly-varying mean flow leads to the presence of so-called critical layers, with their own associated problems.

Very little work has included viscosity in such an analysis, which is the underlying reason for the existence of the boundary layer in the first place. This paper builds on the work of Aurégan, Starobinski & Pagneux (JASA 2001), who derived asymptotic results for a viscous laminar boundary layer over an acoustic lining in the low-Mach-number limit. They found the Myers boundary condition to be applicable only in the high-frequency limit, while the low-frequency limit led to continuity of normal mass-flux. Their asymptotics are here confirmed via a different method, and extended to non-small mean-flow Mach numbers, for which new behaviour is seen. The viscous equations are shown to be regular across the critical layers at which the inviscid equations become singular. Asymptotics are presented that shown the Myers boundary condition is correct in the high-frequency limit only in certain sectors of the frequency- and wave-number planes, and connections are made between this behaviour and the inviscid critical layers.

I. Introduction

The effect of a vanishingly-thin nonviscous boundary layer is know to lead to the so-called Myers boundary condition of continuity of normal displacement.[1–3] Recently there have been several reports on issues of stability when applying the Myers boundary condition to an acoustically-lined duct with flow.[4–9] However, owing to convenience and a lack of any alternative, the Myers boundary condition is still widely used, with any instability artifacts being removed by artificial smoothing.[9–14] In the frequency domain, the problem of instability becomes that of choosing the direction of propagation of modes.[7, 15–17] As a numerical example in the frequency domain, using a pseudo-time method to converges to a solution,[18] it is unclear which of the many potential solutions is converged to, and whether that is the causal one.

In the last couple of years, efforts have been made to resolve these issues by including a nonuniform mean flow that satisfies the no-slip boundary condition at the wall,[19–21] using the Pridmore-Brown equation,[22] since such profiles do not exhibit the possible hydrodynamic instability mode present with slipping mean flow.[17] However, these models introduce their own problems, such as the singularity in the Pridmore-Brown

---

[*]Research Fellow, Department of Applied Mathematics & Theoretical Physics, University of Cambridge, Centre for Mathematical Sciences, Wilberforce Road, Cambridge CB3 0WA, United Kingdom. AIAA member.

equation at the so-called critical layer, and the associated continuous spectrum. To the author's knowledge, the stability of sheared inviscid flow over an acoustic lining has not been studied.

Introducing viscosity into the model, the vanishingly-thin boundary layer limit (for a laminar boundary layer of small mean-flow Mach number and small temperature change) has been shown to be nonuniform,[23] with continuity of normal particle displacement or continuity of normal mass flux obtained in appropriate limits depending on the ratio of the acoustic and mean-flow boundary layer thicknesses. These limits correspond, for everything else being fixed, with low- and high-frequency limits. Adding weight to this, last year remarkably good agreement was shown between the experimental results from NASA Langley[24] and a linearized Navier–Stokes code.[25] These results suggest that viscosity in the boundary layer plays an important role in the behaviour of acoustically-lined ducts. This is not surprising, since viscosity is the fundamental reason for the existence of the boundary layer in the first place.

II.   Governing equations

A.   Geometry and nondimensionalization

We consider flow along a cylindrical duct, possibly with lined or oscillating walls, as shown in figure 1. Lengths are nondimensionalized based on a length scale ℓ^* (* denotes a dimensional variable), velocities
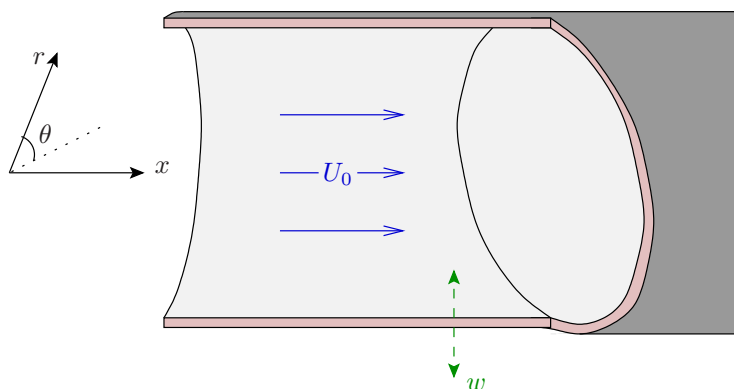

Figure 1.   The geometry considered here, of uniform flow along a cylindrical duct.

based on a reference sound speed c_0^*, and densities based on a reference density ρ_0^*. In what follows, ℓ^* will be taken as the radius of the cylindrical duct, and c_0^* and ρ_0^* will be taken as the speed of sound and density of the mean flow along the centre of the duct. Based on this nondimensionalization, dimensionless quantities are shown in table 1. Note that this nondimensionalization gives the mean-flow centreline pressure

Density	$\rho^* = \rho_0^*\rho$	Pressure & viscous stress	$p^* = c_0^{*2}\rho_0^* p$
Velocity	$\boldsymbol{u}^* = c_0^*\boldsymbol{u}$	Dynamic viscosity (shear & bulk)	$\mu^* = c_0^*\ell^*\rho_0^*\mu$
Distance	$x^* = \ell^* x$	Thermal conductivity	$\kappa^* = c_0^*\ell^*\rho_0^* c_p^*\kappa$
Time	$t^* = \ell^*/c_0^* t$	Temperature	$T^* = c_0^{*2}/c_p^* T$
Entropy	$s^* = c_p^* s$		

Table 1.   Nondimensionalization used, based on a lengthscale ℓ^*, velocity c_0^*, density ρ_0^*, and specific heat at constant pressure c_p^*.

as $p_0 = 1/\gamma$ and the mean-flow temperature as $T_0 = 1/(\gamma - 1)$, where $\gamma = c_p^*/c_v^*$ is the ratio of specific heats.

Six dimensionless numbers govern the flow's behaviour, of which all but one are independent. These are given in table 2. The reference velocity U_0^* is taken as the mean-flow velocity along the centreline. This gives the nondimensional centreline viscosity as $\mu_0 = 1/\text{Re}$, the nondimensional centreline thermal conductivity as $\kappa_0 = 1/\text{Pe}$, and the nondimensional centreline velocity as $U_0 = M$. Note that the Reynolds number Re

	Formula	Typical value
Mach number	$M = U_0^*/c_0^*$	0.5
Reynolds number	$\mathrm{Re} = c_0^*\ell^*\rho_0^*/\mu_0^*$	2.6×10^7
Peclet number	$\mathrm{Pe} = c_0^*\ell^*\rho_0^*c_p^*/\kappa_0^*$	1.8×10^7
Prandtl number	$\mathrm{Pr} = \mathrm{Pe}/\mathrm{Re} = \mu_0^*c_p^*/\kappa_0^*$	0.7
Ratio of bulk to shear viscosity	$\mu_0^{\mathrm{B}} = \mu_0^{\mathrm{B}*}/\mu_0^*$	0.7
Ratio of specific heats	$\gamma = c_p^*/c_v^*$	1.4

Table 2. **Dimensionless numbers.** U_0^* **is a reference fluid flow speed,** μ_0^* **a reference shear viscosity,** $\mu_0^{\mathrm{B}*}$ **a reference bulk viscosity, and** κ_0^* **a reference thermal conductivity. The typical values are those of an aeroengine intake during takeoff.**

is based on the sound speed, not on the flow speed. For air in a typical aeroengine intake at takeoff, typical values of these dimensionless parameters are given in table 2, based on viscosity data for N_2 from.[26]

B. Full viscous compressible equations

The full equations for viscous compressible flow, after the nondimensionalization given in table 1, are:[27] conservation of mass

$$\frac{\partial \rho}{\partial t} + \boldsymbol{\nabla} \cdot (\rho \boldsymbol{u}) = 0; \tag{1a}$$

conservation of momentum

$$\rho \frac{\mathrm{D}\boldsymbol{u}}{\mathrm{D}t} = -\boldsymbol{\nabla} p + \boldsymbol{\nabla} \cdot \sigma, \tag{1b}$$

where $\mathrm{D}/\mathrm{D}t \equiv \partial/\partial t + \boldsymbol{u} \cdot \boldsymbol{\nabla}$, and the viscous stress tensor is given by

$$\sigma_{ij} = \mu \left(\frac{\partial u_i}{\partial x_j} + \frac{\partial u_j}{\partial x_i} \right) + \left(\mu^{\mathrm{B}} - \frac{2}{3}\mu \right) \delta_{ij} \boldsymbol{\nabla} \cdot \boldsymbol{u}; \tag{1c}$$

conservation of energy, in the form of entropy

$$\rho T \frac{\mathrm{D}s}{\mathrm{D}t} = \sigma_{ij} \frac{\partial u_i}{\partial x_j} + \boldsymbol{\nabla} \cdot \left(\kappa \boldsymbol{\nabla} T \right) \tag{1d}$$

or temperature

$$\rho \frac{\mathrm{D}T}{\mathrm{D}t} = \frac{\mathrm{D}p}{\mathrm{D}t} + \sigma_{ij} \frac{\partial u_i}{\partial x_j} + \boldsymbol{\nabla} \cdot \left(\kappa \boldsymbol{\nabla} T \right); \tag{1e}$$

and the equation of state for a perfect gas

$$s = \frac{1}{\gamma} \log \left(\frac{\gamma p}{\rho^\gamma} \right), \qquad\qquad T = \frac{\gamma}{\gamma - 1} \frac{p}{\rho}. \tag{1f}$$

For the range of temperatures and pressures to be considered here, we may take the dynamic shear viscosity μ, the bulk viscosity μ^{B}, and the thermal conductivity κ to be linear in the temperature and independent of the pressure.[26] Hence, we set

$$\mu = (\gamma - 1)T\mu_0 \qquad\qquad \mu^{\mathrm{B}} = (\gamma - 1)T\mu_0^{\mathrm{B}} \qquad\qquad \kappa = (\gamma - 1)T\kappa_0. \tag{1g}$$

While this variation may seem insignificant, and is often neglected (for example by Ref. 23), when the equations are linearized it introduces perturbations that are of a comparable size to the acoustic perturbation.

American Institute of Aeronautics and Astronautics Paper 2009-3241

III. Mean flow cylindrical Blasius boundary layer

We consider a fluid-containing cylinder (of radius 1) whose axis is along the x-axis. Across the majority of the duct the mean flow is uniform with pressure $1/\gamma$, temperature $1/(\gamma-1)$, density 1, and velocity $M\boldsymbol{e_x}$. At the boundary, a boundary layer exists of characteristic width $\delta \ll 1$. We now make the change of variable

$$r = 1 - \delta y, \qquad\qquad \boldsymbol{u} = u(x,y)\boldsymbol{e_x} - \delta v_1(x,y)\boldsymbol{e_r} \qquad\qquad \delta^2 = \mu_0 = 1/\mathrm{Re},$$

this choice of scaling being made so as to scale-out the viscosity from the equations. Henceforth, we will use a subscript to denote differentiation, so that, for example, $\partial\rho/\partial t$ becomes ρ_t.

The θ-momentum equation is identically zero. The axial-momentum equation and the temperature equation both balance, since we chose $\delta^2/\mu = O(1)$. The r-momentum equation then implies that $p_y = O(1/\delta^2)$, so that $p = 1/\gamma + \delta^2 p_1(x,y)$. To leading order, therefore, $1/\rho = (\gamma - 1)T$, and the governing equations become

$$\left(\rho u\right)_x + \left(\rho v_1\right)_y = 0, \tag{2a}$$

$$\rho\left(u u_x + v_1 u_y\right) = \left(\tfrac{\mu}{\delta^2} u_y\right)_y \tag{2b}$$

$$\rho\left(u T_x + v_1 T_y\right) = \left(\tfrac{\kappa}{\delta^2} T_y\right)_y + \tfrac{\mu}{\delta^2}(u_y)^2. \tag{2c}$$

We solve this using the standard compressible Blasius boundary layer method.[28] We first introduce a streamfunction ψ, so that $\rho u = \psi_y$ and $\rho v_1 = -\psi_x$. Introducing the similarity variable ζ,

$$\sqrt{M}\frac{y}{\sqrt{x}} = \int_0^\zeta 1 + \tfrac{\gamma-1}{2}M^2\tau(q)\,\mathrm{d}q \qquad\qquad \psi = \sqrt{M}\sqrt{x}f(\zeta) \qquad\qquad T = \tfrac{1}{\gamma-1} + \tfrac{1}{2}M^2\tau(\zeta).$$

gives

$$ff'' + 2f''' = 0, \qquad\qquad \tau' = -2\mathrm{Pr}(f'')^{\mathrm{Pr}}\int_0^\zeta (f''(q))^{2-\mathrm{Pr}}\,\mathrm{d}q, \tag{3}$$

where $'$ denotes $\mathrm{d}/\mathrm{d}\zeta$, with boundary conditions

$$\begin{aligned} f'(\zeta) &\to 1 \\ \tau(\zeta) &\to 0 \end{aligned} \quad \text{as } \zeta \to \infty \qquad\qquad f'(0) = f(0) = 0.$$

Equation (3) is the classical Blasius boundary layer equation for incompressible fluid flow over a semi-infinite plate. All of this has been derived correct to leading order, so that errors are of $O(\delta)$. Note that all effects of the curvature of the cylinder wall have been neglected, as these occur at $O(\delta)$.

The solution for f from (3) was calculated numerically using a fourth-order finite difference iterative method, following which τ was calculated by numerically integrating the right hand side of (3). Typically, $f(\zeta)$ was calculated using 10^4 equally spaced values of ζ in the range $[0, 11]$, which was found to be suitably accurate for the acoustic calculations performed later. An example of the boundary layer calculated is shown in figure 2.

A. Parallel flow assumption

To the author's knowledge, all analyses of acoustics in acoustically lined ducts have assumed a locally parallel flow profile.[19–21, 23, 29] We now make the same assumption of a parallel boundary layer flow, so that we assume

$$v_1 = 0 \qquad\qquad \frac{\partial u}{\partial x} = 0 \qquad\qquad \frac{\partial T}{\partial x} = 0.$$

This assumption may be justified by expanding $x = x_0 + \Delta x$ with $\Delta x/x_0 \ll 1$ and neglecting terms of $O(\Delta x/x_0)$. Noting that $v_1 = O(1/\sqrt{x_0})$, we also require $x_0 \gg 1$ in order to neglect v_1.

This means that there are two boundary layer parameters we can use to alter the boundary layer thickness. The first is the Reynolds number since the boundary lengthscale over which viscosity is important, used to rescale r to y above, is $\delta = \mathrm{Re}^{-1/2}$. Provided the Reynolds number is large, the actual numerical value is never used in this paper, since we are only concerned with the leading-order behaviour, and so Re is either assumed infinite (within the uniform flow in the centre of the duct) or is scaled out (within the boundary layer). The second parameter is the downstream location x, since the Blasius boundary layer is a function of $y/\sqrt{x}$ (refer to figure 2 above).
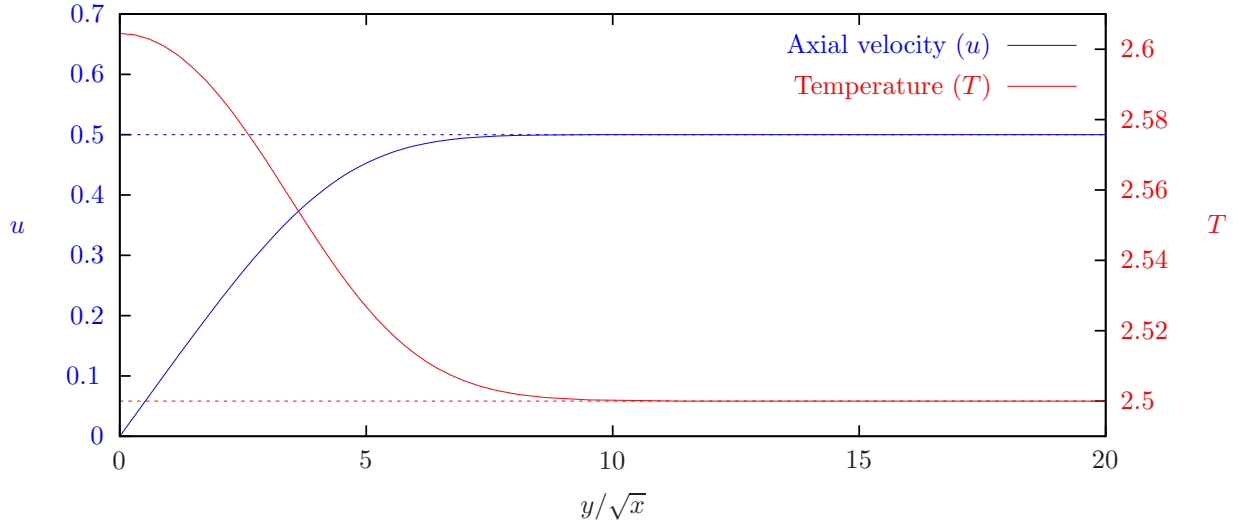
Figure 2. The compressible Blasius boundary layer profile for $M = 0.5$, $\mathrm{Pr} = 0.7$ and $\gamma = 1.4$. Scales are nondimensionalized axial velocity u (left) and temperature T (right).

IV. Linearized sound

A.   Linearized sound in uniform flow

We now consider a small time-dependent perturbation to a steady laminar boundary layer flow. Outside the boundary layer, the mean flow is assumed to be axial and uniform, with nondimensionalized velocity M, the Mach number. We assume that viscosity is negligible within this uniform flow. Linearizing, we write, for example, $\rho + \tilde{\rho}$ for the density, where ρ is as derived above and $\tilde{\rho}$ is the acoustic perturbation, of small magnitude. Introducing an acoustic velocity potential ϕ, the standard convected acoustic perturbation equation (see, e.g., Ref. 30) with the nondimensionalization used here is

$$\left(\frac{\partial}{\partial t} + M\frac{\partial}{\partial x}\right)^2 \phi - \nabla^2\phi = 0, \qquad \tilde{p} = \tilde{\rho} = -\left(\frac{\partial}{\partial t} + M\frac{\partial}{\partial x}\right)\phi, \qquad \tilde{\boldsymbol{u}} = \boldsymbol{\nabla}\phi.$$

All time-dependent perturbations are assumed to have $\exp\{\mathrm{i}\omega t - \mathrm{i}kx - \mathrm{i}m\theta\}$ dependence, giving modal solutions in terms of Bessel's functions,

$$\phi = AJ_m(\alpha r)\exp\{\mathrm{i}\omega t - \mathrm{i}kx - \mathrm{i}m\theta\}, \qquad \alpha^2 = (\omega - Mk)^2 - k^2.$$

The $\exp\{\cdots\}$ factor will be implicitly assumed from here on.

At the cylinder boundary $(r = 1)$, the normal velocity (referred to as $\tilde{v}_\infty$ because of what follows) and the pressure acting on the boundary $\tilde{p}$ are

$$\tilde{v}_\infty = A\alpha J_m'(\alpha), \qquad\qquad \tilde{p} = -\mathrm{i}(\omega - Mk)AJ_m(\alpha). \qquad (4)$$

The boundary physics relates these two quantities, giving the dispersion relation for the allowable values of k (given ω). We are interested in this paper in how the presence of a boundary layer affects this relation.

B.   Linearized sound within the boundary layer

The analysis in this section is general and independent of the boundary layer profile used, assuming that the boundary layer is axial and parallel. Later in this paper, these equations will be applied to the Blasius profile derived above. The method followed here is similar to that of Ref. 23. Setting $\boldsymbol{u} = (u + \tilde{u}, -\delta(v + \tilde{v}), \tilde{w})$ and neglecting terms quadratic in the perturbation amplitude or of order $O(\delta)$ gives

$$\mathrm{i}(\omega - uk)\tilde{\rho} + v\tilde{\rho}_y + \rho(\tilde{v}_y - \mathrm{i}k\tilde{u} - \mathrm{i}m\tilde{w}) + \tilde{\rho}(u_x + v_y) + \rho_x\tilde{u} + \rho_y\tilde{v} = 0,$$

$$\mathrm{i}(\omega - uk)\tilde{u} + v\tilde{u}_y + \tilde{u}u_x + \tilde{v}u_y + \frac{\tilde{\rho}}{\rho}\left(uu_x + vu_y\right) = \tfrac{1}{\rho}\mathrm{i}k\tilde{p} + \tfrac{\gamma-1}{\rho}\left(T\tilde{u}_y + \tilde{T}u_y\right)_y,$$

$$\tilde{p}_y = O(\delta^2)$$

$$\rho\Big(\mathrm{i}(\omega - uk)\tilde{w} + v\tilde{w}_y\Big) = \mathrm{i}m\tilde{p} + (\gamma - 1)\left(T\tilde{w}_y\right)_y$$

$$\rho\Big(\mathrm{i}(\omega - uk)\tilde{T} + v\tilde{T}_y + \tilde{u}T_x + \tilde{v}T_y\Big) + \tilde{\rho}\Big(uT_x + vT_y\Big)$$

$$= \mathrm{i}(\omega - uk)\tilde{p} + \tfrac{\gamma-1}{\mathrm{Pr}}\left(\tilde{T}T_y + T\tilde{T}_y\right)_y + (\gamma - 1)\Big(\tilde{T}(u_y)^2 + 2Tu_y\tilde{u}_y\Big),$$

$$\tilde{s} = \tilde{p} - \tilde{\rho}/\rho = (\gamma - 1)\big(\rho\tilde{T} - \tilde{p}\big), \qquad\qquad (\gamma - 1)\rho^2\tilde{T} = \gamma\rho\tilde{p} - \tilde{\rho}.$$

Hence, as for the steady mean flow, $\tilde{p}$ is constant across the boundary layer to order $O(\delta^2)$.

Balancing the orders of these terms and matching the boundary layer solution with the acoustic solution outside the boundary layer gives $\tilde{p}$ and $\tilde{w}$ being $O(1)$ while $\tilde{u}$, $\tilde{v}$, $\tilde{\rho}$ and $\tilde{T}$ are $O(1/\delta)$. These assumptions give, to leading order,

$$\mathrm{i}(\omega - uk)\tilde{T} + T_y\tilde{v} - T\tilde{v}_y + \mathrm{i}kT\tilde{u} = 0, \tag{5a}$$

$$\mathrm{i}(\omega - uk)\tilde{u} + \tilde{v}u_y = (\gamma - 1)^2 T\left(T\tilde{u}_y + \tilde{T}u_y\right)_y, \tag{5b}$$

$$\mathrm{i}(\omega - uk)\tilde{T} + \tilde{v}T_y = (\gamma - 1)^2 T\left[\tfrac{1}{\mathrm{Pr}}\big(\tilde{T}T\big)_{yy} + \tilde{T}(u_y)^2 + 2Tu_y\tilde{u}_y\right], \tag{5c}$$

$$\tilde{\rho} = -(\gamma - 1)\rho^2\tilde{T} = -\rho\tilde{s}. \tag{5d}$$

Introducing the normal particle displacement $\tilde{xi} = \tilde{v}/\big(\mathrm{i}(\omega - uk)\big)$ and combining these equations gives

$$\tilde{\xi}_y = \frac{(\gamma - 1)^2}{\mathrm{i}(\omega - uk)}\left[\tfrac{1}{\mathrm{Pr}}\big(T\tilde{T}\big)_{yy} + \tilde{T}(u_y)^2 + 2Tu_y\tilde{u}_y + \frac{\mathrm{i}kT}{\mathrm{i}(\omega - uk)}\big(T\tilde{u}_y + \tilde{T}u_y\big)_y\right], \tag{6}$$

which gives the change in normal particle displacement across the boundary layer as an integral of dispersive terms. Equation (6) is the equivalent of equation (14) of Ref. 23. If we were to ignore dissipative effects within the boundary layer, the right hand side of (6) would be zero, and so $\tilde{\xi}$ would be constant across the boundary layer; that is, we would recover the Myers boundary condition of continuity of normal particle displacement.[1–3] Ref. 23 used this result as the basis of their asymptotics. Here, we will instead derive our asymptotics from (5).

For an acoustically-lined boundary which is fixed and permeable, the boundary conditions on the acoustic perturbation are

$$\tilde{u}(0) = 0, \qquad\qquad \tilde{v}(0) = -\tilde{v}_0/\delta, \qquad\qquad \tilde{T}(0) = 0,$$

$$\tilde{u}(y) \to 0, \qquad\qquad \tilde{v}(y) \to -\tilde{v}_\infty/\delta, \qquad\qquad \tilde{T}(y) \to 0, \qquad\qquad \text{as } y \to \infty.$$

where $\tilde{v}_0$ is the velocity of fluid flowing through the permeable boundary and $\tilde{v}_\infty$ is the apparent boundary velocity seen by the acoustic perturbation outside the boundary layer (this is why the notation $\tilde{v}_\infty$ was used in (4) above). The boundary condition for $\tilde{T}$ assumes the boundary to have a far higher thermal conductivity than the fluid. The solution will necessarily have $\tilde{v}$, $\tilde{T}$, and $\tilde{u}$ of $O(1/\delta)$, as stated earlier, leading to the stated boundary conditions as $y \to \infty$.

C. Application to acoustic lining

The response of the acoustic lining is governed by its impedance, $Z = \tilde{p}/\tilde{v}_0$, where a pressure $\tilde{p}\exp\{i\omega t\}$ yields a fluid velocity through the lining $\tilde{v}\exp\{i\omega t\}$. This gives the boundary condition

$$\tilde{v}_0 = \frac{\tilde{p}}{Z}.$$

We would like to know the effective impedance Z_{eff} seen by the mean flow, given by

$$Z_{\text{eff}} = \frac{\tilde{p}}{\tilde{v}_\infty} = Z\frac{\tilde{v}_0}{\tilde{v}_\infty}.$$

If we were to assume continuity of normal particle displacement across the boundary layer, we would find $\tilde{v}_\infty = (1 - Mk/\omega)\tilde{v}_0$, leading to the impedance boundary condition for the acoustics outside the boundary layer

$$Z_{\text{eff}} = Z_{\text{disp}} = \frac{Z}{1 - Mk/\omega}, \tag{7}$$

which is as derived by Eversman & Beckemeyer[1] and Tester.[2] Such a boundary condition is usually applied using the Myers boundary condition[3] directly using Z without considering the intermediary Z_{eff}.

If instead we were to assume continuity of normal mass flux across the boundary layer (as suggested from Ref. 23 in the low-frequency limit) we would find $\tilde{v}_0 = (\gamma - 1)T(0)\tilde{v}_\infty$, leading to the impedance condition for the acoustics outside the boundary layer

$$Z_{\text{eff}} = Z_{\text{mass}} = (\gamma - 1)T(0)Z.$$

Note that $(\gamma - 1) = 1/T(\infty)$ owing to the nondimensionalization used.

In general, we calculate Z_{eff} here without any of these assumptions by numerically calculating $\tilde{v}_0/\tilde{v}_\infty$ from (5), as described in §IV.E below.

D. Boundary conditions at infinity

Let us now assume that the boundary layer velocity and temperature profiles are constant at their mean-flow values for some $y > Y$, so that $u(y) = M$ and $T(y) = 1/(\gamma - 1)$. This is true for the Blasius boundary layer to computational precision for $Y \approx 20\sqrt{x_0}$. Equations (5a–c) simplify and uncouple in this case, to give

$$i(\omega - Mk)(\gamma - 1)\tilde{T} + ik\tilde{u} = \tilde{v}_y, \tag{8a}$$

$$i(\omega - Mk)\tilde{u} = \tilde{u}_{yy}, \tag{8b}$$

$$i(\omega - Mk)\tilde{T} = \tfrac{1}{\text{Pr}}\tilde{T}_{yy}. \tag{8c}$$

For $y > Y$, we have $\tilde{u} = \tilde{u}_\infty \exp\{-\eta y\}$ and $\tilde{T} = \tilde{T}_\infty \exp\{-\sigma\eta y\}$, where $\sigma^2 = \text{Pr}$ and $\eta^2 = i(\omega - Mk)$ and both $\text{Re}(\sigma)$ and $\text{Re}(\eta)$ are positive, for unknown constants $\tilde{u}_\infty$ and $\tilde{T}_\infty$. For $\tilde{u}$ and $\tilde{T}$ to have solutions that decay to zero as $y \to \infty$, we require $i(\omega - Mk)$ to not be both real and negative. For fixed ω, this gives a branch cut in the k-plane along $k = \omega/M - iq$ for $q \geq 0$. It is emphasized that this is different from the inviscid critical layer, which would be in the k-plane along $k = \omega/M + q$ for $q \geq 0$.

E. Numerical solution

Equations (5a–c) were discretized using a fourth-order symmetric finite-difference scheme applied on an equally-spaced set of N points in the interval $y \in [0, Y]$. This yielding a $3N \times 3N$ banded matrix A with less than $48N$ nonzero elements. The boundary conditions at $y = 0$ were specified as $\tilde{u}(0) = \tilde{T}(0) = 0$ and $\tilde{v}(0) = 1$. The solutions for $y > Y$ given in (8c) above were used to give numerical boundary conditions at $y = Y$. These boundary conditions were

$$\tilde{u}_y + \eta\tilde{u} = 0, \qquad\qquad \tilde{T}_y + \sigma\eta\tilde{T} = 0.$$

These initial conditions were encapsulated into a $3N$-dimensional vector $\boldsymbol{b}$, with $b_1 = 1$ and $b_i = 0, i \in [2, 3N]$. The discretized problem was therefore to solve $A\boldsymbol{x} = \boldsymbol{b}$ for the solution $\boldsymbol{x}$, which was performed using the LAPACK ZGBSV routine.[31] After this calculation, (8c) was used to interpolate $\tilde{v}$ at $y = Y$ to $y = \infty$.

Typically, $Y = 20\sqrt{x}$ and $N = 4000$ were used for the results that follow. One solution took about 10ms on a standard desktop computer. Such a fast solution was necessary, since this calculation was used in a Newton–Raphson root-finding iteration to find modal solutions, and was typically solved 20 times per mode.

F. Frobenius expansion about the critical layer

In this subsection, we investigate the behaviour of (5a–c) about a point y_0 at which $\omega - u(y_0)k = 0$. For inviscid shear flows, the point y_0 is referred to as the critical layer.[20] We use the Frobenius method of expanding locally about the potential singularity, and so we set $z = y - y_0$ and pose the expansions for small z

$$\tilde{v} = z^\nu \sum_{n=0}^{\infty} \tilde{v}_n z^n, \qquad \tilde{u} = z^\mu \sum_{n=0}^{\infty} \tilde{u}_n z^n, \qquad \tilde{T} = z^\tau \sum_{n=0}^{\infty} \tilde{T}_n z^n,$$

$$u = \sum_{n=0}^{\infty} u_n z^n, \qquad T = \sum_{n=0}^{\infty} T_n z^n,$$

with nonzero leading coefficients. After some detective work, the leading-order powers (ν, μ, τ) for the five linearly-independent solutions can be deduced; these coefficients are:

Specify	ν	μ	τ	Extra conditions
$\tilde{v}_0 = \tilde{v}(y_0)$	0	2	2	
$\tilde{u}_0 = \tilde{u}'(y_0)$	2	1	2	
$\tilde{T}_0 = \tilde{T}'(y_0)$	3	2	1	
$\tilde{u}_0 = \tilde{u}(y_0)$	1	0	3	$\tilde{u}_1 = 0$
$\tilde{T}_0 = \tilde{T}(y_0)$	1	2	0	$\tilde{T}_1 = 0$

The reason for the extra conditions in the fourth and fifth solutions is that, without these, these solutions would contain an arbitrary multiple of the second and third solutions. Since the set of equations are fifth order in total, these are all the solutions, and they are all regular at the critical layer $z = 0$, equivalently $y = y_0$. We have therefore shown that the inclusion of disipative terms regularizes the singularity in the Pridmore-Brown equations, and so we can expect all our solutions to be smooth.

V. Asymptotics

A. The Low-frequency limit

Rewriting (5a–c) in a convenient form gives

$$\left(\frac{\tilde{v}}{T}\right)_y = \frac{i\omega}{T^2}\left[\left(1 - \frac{uk}{\omega}\right)\tilde{T} + \frac{k}{\omega}T\tilde{u}\right], \tag{9a}$$

$$(T\tilde{u}_y + \tilde{T}u_y)_y - \frac{u_y\tilde{v}}{(\gamma-1)^2 T} = \frac{i\omega}{(\gamma-1)^2 T}\left(1 - \frac{uk}{\omega}\right)\tilde{u}, \tag{9b}$$

$$\tfrac{1}{\mathrm{Pr}}(\tilde{T}T)_{yy} + \tilde{T}(u_y)^2 + 2Tu_y\tilde{u}_y - \frac{T_y\tilde{v}}{(\gamma-1)^2 T} = \frac{i\omega}{(\gamma-1)^2 T}\left(1 - \frac{uk}{\omega}\right)\tilde{T}. \tag{9c}$$

For $y > Y$, we know that

$$\tilde{u} = \tilde{u}_\infty e^{-\eta y}$$

$$\tilde{T} = \tilde{T}_\infty e^{-\sigma \eta y}$$

$$\tilde{v} = \tilde{v}_\infty - \frac{\eta}{\sigma}(\gamma-1)\tilde{T}_\infty e^{-\sigma \eta y} - \frac{ik}{\eta}\tilde{u}_\infty e^{-\eta y}.$$

Considering the low-frequency limit $\omega \to 0$ with $k/\omega = O(1)$, and setting $\bar{\eta}^2 = i(1 - uk/\omega)$ with $\mathrm{Re}\left(\bar{\eta}(\infty)\right) > 0$, expanding the exact result for $y > Y$ in powers of ω gives

$$\tilde{v} = \tilde{v}_\infty - \omega^{1/2}\left[\frac{\bar{\eta}}{\sigma}(\gamma-1)\tilde{T}_\infty + \frac{ik}{\omega\bar{\eta}}\tilde{u}_\infty\right] + \omega y\left[(\gamma-1)\bar{\eta}^2\tilde{T}_\infty + \frac{ik}{\omega}\tilde{u}_\infty\right] + O(\omega^{3/2}),$$

$$\tilde{u} = \tilde{u}_\infty - \omega^{1/2}\bar{\eta}y\tilde{u}_\infty + \tfrac{1}{2}\omega\bar{\eta}^2 y^2\tilde{u}_\infty + O(\omega^{3/2}),$$

$$\tilde{T} = \tilde{T}_\infty - \omega^{1/2}\sigma\bar{\eta}y\tilde{T}_\infty + \tfrac{1}{2}\omega\sigma^2\bar{\eta}^2 y^2\tilde{T}_\infty + O(\omega^{3/2}).$$

We will match the inner solution to this expansion, and so look for an inner solution in powers of $\omega^{1/2}$, so that $\tilde{v} = \tilde{v}_0 + \omega^{1/2}\tilde{v}_1 + \cdots$. Then (9a), to leading order, gives

$$\tilde{v}_0 = (\gamma - 1)T\tilde{v}_\infty,$$

where $\tilde{v}_\infty$ is a constant, chosen to match the outer expansion. This is continuity of normal mass flux across the boundary layer. This result agrees with Ref. 23, who showed conservation of mass flux in the low-frequency small-Mach-number limit. Here, the validity of this observation is extended, since we have not needed to assumed a small Mach number.

The low-frequency analysis may be continued to $\tilde{u}$ and $\tilde{T}$, and to higher orders, but as yet has not yielded a closed-form solution, and so will not be pursued further here.

B. The high-frequency limit

We now attempt to solve (5a–c) in the high frequency limit, using a Multiple Scales method. This is a similar analysis to that used for the Pridmore-Brown equation in Ref. 20. Picking any branch for $\sqrt{\omega}$ and introducing the variables

$$\Gamma = i\left(1 - \frac{uk}{\omega}\right) \qquad\qquad \eta^2 = \frac{\Gamma}{(\gamma - 1)^2 T^2} \qquad \text{with } \mathrm{Re}\left(\sqrt{\omega}\eta(\infty)\right) > 0,$$

we pose the Multiple Scales WKB ansatz

$$\frac{\mathrm{d}}{\mathrm{d}y} = \frac{\partial}{\partial y} + \sqrt{\omega}\eta(y)\frac{\partial}{\partial\theta}.$$

This yields the same system of equations when evaluated along $y = y$ and

$$\theta = \sqrt{\omega}\int_0^y \eta(y')\,\mathrm{d}y'.$$

Moreover, in order to balance terms we find that $\tilde{v} = O(\sqrt{\omega})$, and so we introduce $\tilde{v} = \sqrt{\omega}\tilde{\tilde{v}}$. Substituting this into (5a–c) gives the system of equations

$$\Gamma\tilde{T} - \eta T\tilde{\tilde{v}}_\theta + \frac{ik}{\omega}T\tilde{u} = \frac{T^2}{\sqrt{\omega}}\left(\frac{\tilde{\tilde{v}}}{T}\right)_y, \tag{10a}$$

$$\tilde{u}_{\theta\theta} - \tilde{u} = \frac{\tilde{\tilde{v}}u_y}{\sqrt{\omega}\Gamma} - \frac{(\gamma-1)^2 T}{\sqrt{\omega}\Gamma}\left[T_y\eta\tilde{u}_\theta + 2T\eta\tilde{u}_{\theta y} + T\eta_y\tilde{u}_\theta + \eta u_y\tilde{T}_\theta\right]$$
$$- \frac{(\gamma-1)^2 T}{\omega\Gamma}\left(T\tilde{u}_y + \tilde{T}u_y\right)_y, \tag{10b}$$

$$\frac{1}{\mathrm{Pr}}\tilde{T}_{\theta\theta} - \tilde{T} = \frac{\tilde{\tilde{v}}T_y}{\sqrt{\omega}\Gamma} - \frac{(\gamma-1)^2 T}{\sqrt{\omega}\Gamma}\left[\frac{1}{\mathrm{Pr}}\left(2\eta(T\tilde{T}_\theta)_y + \eta_y T\tilde{T}_\theta\right) + 2Tu_y\eta\tilde{u}_\theta\right]$$
$$- \frac{(\gamma-1)^2 T}{\omega\Gamma}\left[\frac{1}{\mathrm{Pr}}(T\tilde{T})_{yy} + \tilde{T}(u_y)^2 + 2Tu_y\tilde{u}_y\right]. \tag{10c}$$

We now solve this using the series $\tilde{u} = \tilde{u}_0 + \omega^{-1/2}\tilde{u}_1 + \cdots$ on the assumption that $\Gamma \neq 0$ for any y. At $O(1)$, setting $\sigma = \sqrt{\mathrm{Pr}}$, we get

$$\tilde{u}_0 = A_0 e^\theta + B_0 e^{-\theta}, \qquad\qquad \tilde{T}_0 = C_0 e^{\sigma\theta} + D_0 e^{-\sigma\theta},$$

$$\tilde{\tilde{v}}_0 = E_0 + \frac{ik}{\eta\omega}\left(A_0 e^\theta - B_0 e^{-\theta}\right) + \frac{\Gamma}{\sigma\eta T}\left(C_0 e^{\sigma\theta} - D_0 e^{-\sigma\theta}\right).$$

At $O(\omega^{-1/2})$, preventing a "secular"[a] term arising in (10b) gives

$$\left(\Gamma\eta T A_0^2\right)_y = 0, \qquad\qquad \left(\Gamma\eta T B_0^2\right)_y = 0,$$

---

[a]This term is technically not secular, since the exponentials are exponentially increasing and decreasing. However, taking y to be complex and such that $\mathrm{Re}(\Delta\theta) = 0$ justifies this being a secular term.

and solving for $\tilde{u}_1$ gives

$$\tilde{u}_1 = A_1 \mathrm{e}^\theta + B_1 \mathrm{e}^{-\theta} - \frac{E_0 u_y}{\Gamma} - \frac{u_y}{\sigma \eta T} \left(C_0 \mathrm{e}^{\sigma\theta} - D_0 \mathrm{e}^{-\sigma\theta} \right).$$

Similarly, preventing a secular term arising in (10c) gives

$$\left(\eta T {C_0}^2 \right)_y = 0, \qquad\qquad\qquad \left(\eta T {D_0}^2 \right)_y = 0,$$

and solving for $\tilde{T}_1$ (assuming $\mathrm{Pr} \neq 1$) gives

$$\tilde{T}_1 = C_1 \mathrm{e}^{\sigma\theta} + D_1 \mathrm{e}^{-\sigma\theta} - \frac{E_0 T_y}{\Gamma} + \frac{\mathrm{Pr}}{(1-\mathrm{Pr})\eta} \left(\frac{ik T_y}{\omega \Gamma} - 2u_y \right) \left(A_0 \mathrm{e}^\theta - B_0 \mathrm{e}^{-\theta} \right).$$

Finally, preventing a secular term arising in (10a) gives

$$\left(\frac{E_0}{\Gamma} \right)_y = 0 \qquad\qquad \Rightarrow \qquad\qquad E_0 = \Gamma \Xi_0,$$

which is continuity of normal particle displacement Ξ_0. This is as expected from Ref. 23, again extending their result to non-small Mach numbers. Solving for $\tilde{v}_1$ gives

$$\tilde{v}_1 = E_1 + \frac{ik}{\eta\omega} \left(A_1 \mathrm{e}^\theta - B_1 \mathrm{e}^{-\theta} \right) + \frac{\Gamma}{\sigma\eta T} \left(C_1 \mathrm{e}^{\sigma\theta} - D_1 \mathrm{e}^{-\sigma\theta} \right) + \frac{(\gamma-1)^2}{\mathrm{Pr}\Gamma} \left((T\Gamma C_0)_y \mathrm{e}^{\sigma\theta} + (T\Gamma D_0)_y \mathrm{e}^{-\sigma\theta} \right)$$

$$+ \left[\frac{1}{(1-\mathrm{Pr})\eta T} \left(\frac{ik T_y}{\omega} - 2\mathrm{Pr} u_y \Gamma \right) - \frac{ik}{\eta\omega} \frac{\partial}{\partial y} \right] \left((A_0/\eta) \mathrm{e}^\theta + (B_0/\eta) \mathrm{e}^{-\theta} \right).$$

We may now apply the boundary conditions to the leading order solution, to find that $A_0 = B_0 = C_0 = D_0 = 0$.

At $O(\omega^{-1})$, exactly the same secularity conditions as above occur. However, now the boundary condition for $\tilde{u}_1(0) = 0$ implies $B_1(0) = \Xi_0 u_y(0)$, while the other boundary conditions imply $A_1 = C_1 = D_1 = E_1 = 0$. Putting all this together, our high-frequency asymptotic solution is

$$(1 - Mk/\omega)\tilde{v}/\tilde{v}_\infty = 1 - uk/\omega - \frac{1}{\sqrt{\omega}} \frac{u_y(0)k/\omega}{\eta(1 - uk/\omega)^{3/4}} \mathrm{e}^{-\theta} + O(\omega^{-1}), \tag{11a}$$

$$(1 - Mk/\omega)\tilde{u}/\tilde{v}_\infty = \frac{i}{\omega} \left[u_y - u_y(0)(1 - uk/\omega)^{-3/4} \mathrm{e}^{-\theta} \right] + O(\omega^{-3/2}), \tag{11b}$$

$$(1 - Mk/\omega)\tilde{T}/\tilde{v}_\infty = O(\omega^{-3/2}), \tag{11c}$$

giving

$$Z_{\mathrm{eff}} = \frac{Z}{1 - Mk/\omega} \left[1 - \frac{u_y(0)k}{\eta\omega^{3/2}} + O(\omega^{-1}) \right]. \tag{12}$$

Equation 12 gives the first-order correction to the Myers impedance given in (7). It is interesting to note that this correction term depends only on $u_y(0)$, and is otherwise independent of the boundary layer profiles $u(y)$ and $T(y)$.

Note that the multiple scales asymptotics (11) has a caustic for values of y for which $1 - u(y)k/\omega = 0$, which is exactly the critical layer. An inner scaling region is needed to correct the asymptotics in this case. This situation is drastically different from the inviscid asymptotics of the Pridmore-Brown equation,[20] since the Pridmore-Brown equation is singular at the critical layer, whereas we have shown previously that (5) are regular everywhere, even at this critical layer. The caustic is therefore a singularity of the asymptotics, rather than the underlying equations, and is alleviated by considering an inner scaling region. This is not pursued further here.

VI.   Results

A.   Comparison of boundary layer numerics with Myers boundary condition

This section has a dual purpose: to present some numerical results (as described by equations 5); and to compare the numerical results with what would have been attained assuming continuity of normal particle displacement, which is the so-called Myers boundary condition.

For a boundary with impedance Z, the effect of the boundary layer is to present the effective boundary impedance Z_{eff} to the mean flow acoustics. Assuming continuity of normal particle displacement, the effective boundary impedance would be Z_{disp}. To compare the two, we plot $Z_{\text{eff}}/Z_{\text{disp}}$, which is given by

$$Z_{\text{eff}}/Z_{\text{disp}} = (1 - Mk/\omega)\frac{\tilde{v}_0}{\tilde{v}_\infty}.$$

This is plotted in the k-plane in figure 3 for parameters applicable to aeroengine intakes: $\omega = 31$, $M = 0.5$. Throughout all the results presented here, $\text{Pr} = 0.7$ and $\gamma = 1.4$. The thickness parameter $x = 1$ was chosen for the thickness of the boundary layer in an aeroengine intake, since this represents the thickness of a laminar Blasius boundary layer one duct radius downstream of the intake lip. The branch cut predicted in §IV.D is clearly visible. The majority of the k-plane is seen to have $Z_{\text{eff}}/Z_{\text{disp}} \approx 1$, which is as predicted[1, 2, 23] and agrees with the high-frequency asymptotics of §V.B. However, for $\text{Im}(k) < 0$ and behind the branch cut ($\text{Re}(k) > 62$) the continuity of normal particle displacement is seen not to hold.

The critical layer would be along the real k-axis for $k > 62$; however, as predicted in §IV.F, no singularities are present there.

The effect that this change in the effective impedance has on the duct modes is shown in figure 4, for the same parameters as figure 3 and with a boundary impedance of $Z = 2 + i$. The background colours are from figure 3. The majority of duct modes lie in the region well-predicted by the Myers boundary condition. The potential hydrodynamic-instability surface mode[17, 32] in the upper-right of the k-plane has moved by a nontrivial amount. Most important, however, are three new modes inhabiting the region of the k-plane where the Myers boundary condition is invalid.

B. Comparison of numerics and high-frequency asymptotics

In this section, we will compare the numerics, the high-frequency asymptotics derived in §V.B, and the solution assuming continuity of normal particle displacement, for $\tilde{v}$ across the boundary layer for four different points in the k-plane. These are: $k = 1$, for which $\text{Re}(k) < \omega/M$, shown in figure 5; $k = 51 + 5i$, for which $\text{Re}(k)$ is close to $\omega/M = 62$ but $\text{Im}(k) > 0$, shown in figure 6; $k = 63i$, for which $\text{Re}(k)$ is close to but greater than $\omega/M = 62$ and $\text{Im}(k) = 0$, so that k lies on the "critical layer", shown in figure 7; and $k = 70 - 70i$, for which $\text{Re}(k) > \omega/M = 62$ and $\text{Im}(k) < 0$, so that k lies in the region for which the Myers boundary condition is invalid, shown in figure 8.

Figures 5 and 6 show that the asymptotics of §V.B and the numerics for $\tilde{v}$ coincide well, and that the shape predicted by the asymptotics of §V.B fits better with the numerics than does the Myers boundary condition assumption of continuity of normal particle displacement. Figure 7 shows the behaviour of the asymptotics across the caustic (located at the same place as the "critical layer"), after which the numerics and the asymptotics diverge. This is due to the lack of an inner scaling region to properly account for the caustic in the asymptotics. Note that the numerical solution is smooth across the "critical layer", as predicted by in §IV.F.

Figure 8 also shows a disagreement between the numerics and the asymptotics, especially for $y \to \infty$. The asymptotics is predicting the correct kind of behaviour, which is highly oscillatory and an order of magnitude greater than at either $y = 0$ or $y \to \infty$. This behaviour is caused by the multiple scales WKB coefficient $\eta(y)$, which is defined so that $\text{Re}(\eta(\infty)) > 0$, going around a branch point so that $\text{Re}(\eta(y)) < 0$ for $y < y_0$ for some y_0. Doing so invalidates the ordering of small terms in the asymptotic expansion, since $e^{-\theta}$ can no-longer be considered to be at most $O(1)$. This behaviour could be indicative of some sort of turbulence being generated within the boundary layer. The continuity of normal displacement assumption is clearly incorrect in this case.

The behaviour at high frequency is sketched in figure 9. In the k-plane, the region of interesting non-Myersian behaviour due to $\text{Re}(\eta(y)) < 0$ for y in some region can be shown to be bounded by the branch cut $k = \omega/M - iq$ for $q > 0$ and the caustic $k = q\omega/M$ for $q > 1$ (also referred to here as the "critical layer"). In the ω-plane, these two boundaries map to $\omega = kM + iq$ for $q > 0$ and $\omega = qkM$ for $0 < q < 1$ respectively. The third boundary to the region of interesting behaviour in the ω-plane is the "Growth Limit" line $\omega = iq$ for $q > 0$, since it can be shown that $y_0 \to \infty$ as $\text{Re}(\omega) \to 0^+$ with $\text{Im}(\omega) > 0$.

In conclusion, the interesting behaviour is seen in the k-plane in an infinite quarter plane bounded by the caustic and the branch cut, and in the ω-plane in a strip bounded by the caustic, the branch cut, and the positive imaginary axis. Within this interesting region, continuity of normal particle displacement does not hold. All of this analysis is, however, limited to high frequencies.
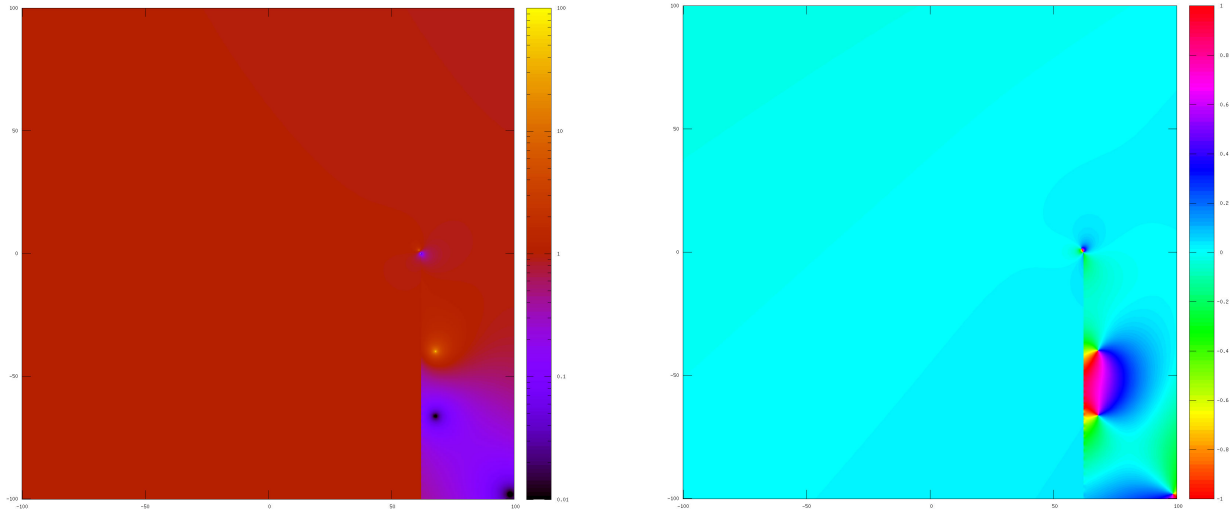
Figure 3. $Z_{\text{eff}}/Z_{\text{disp}}$ **in the** k**-plane. Left:** $|Z_{\text{eff}}/Z_{\text{disp}}|$ **with logarithmic scale** $[10^{-2}, 10^2]$. **Right:** $\arg(Z_{\text{eff}}/Z_{\text{disp}})$. $\omega = 31$, $M = 0.5$, $\text{Pr} = 0.7$, $\gamma = 1.4$, $x = 1$.
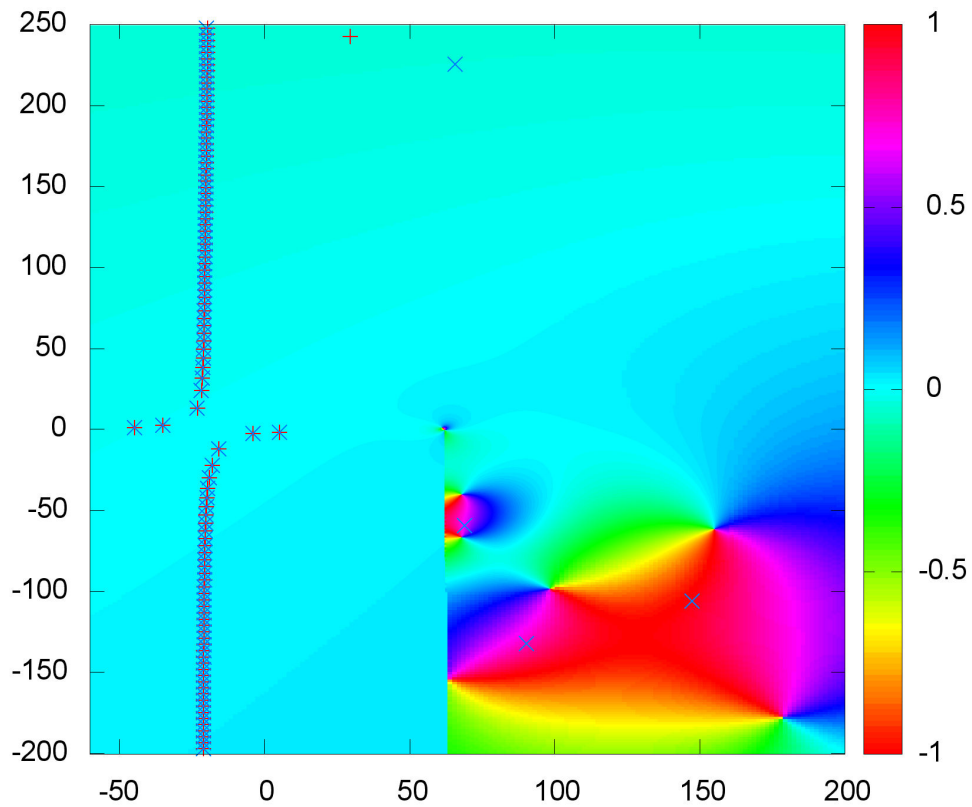

Figure 4. **Effects of the boundary layer on modes at high frequency. Plotted is** $\arg(Z_{\text{eff}}/Z_{\text{disp}})$ **(colour background), without boundary layer modes** (+)**, and with boundary layer modes** (×)**.** $\omega = 31$, $m = 24$, $M = 0.5$, $\text{Pr} = 0.7$, $\gamma = 1.4$, $x = 1$, $Z = 2 + \text{i}$.
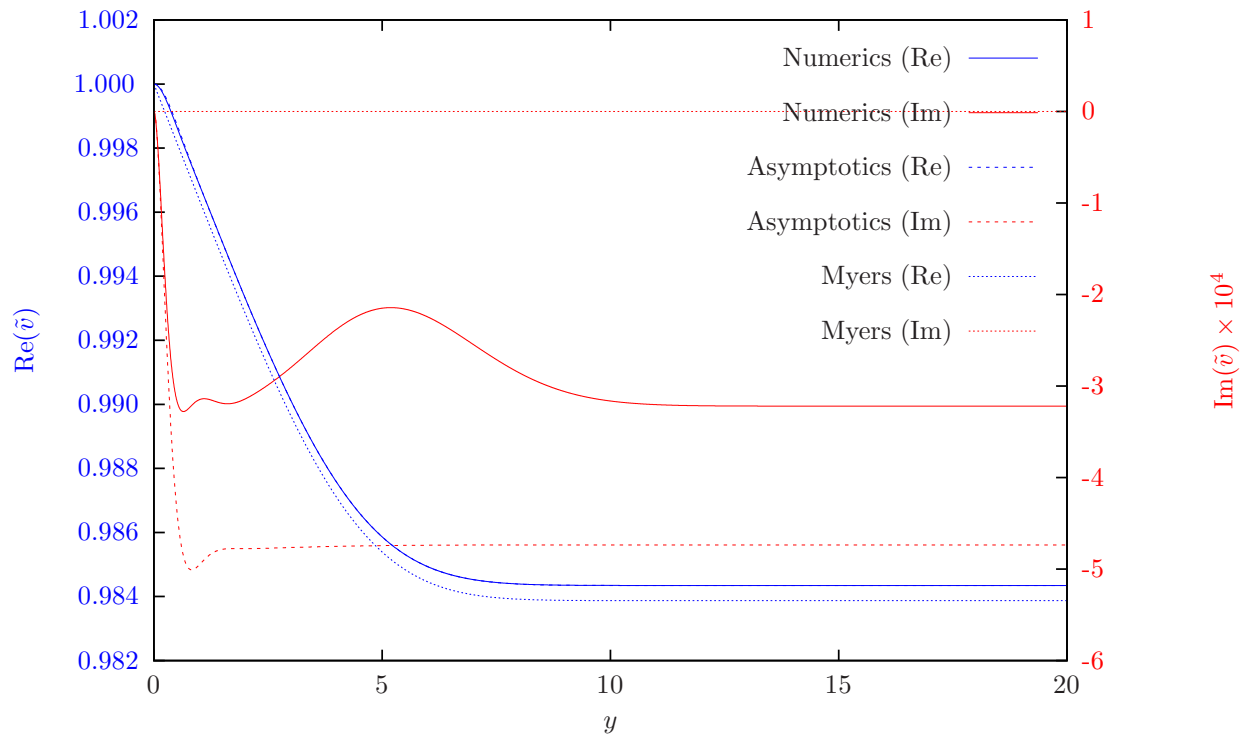
Figure 5. **Comparison of numerics and high-frequency asymptotics for** $\tilde{v}$ **for small** k. $k = 1$, $\omega = 31$, $M = 0.5$, $\mathrm{Pr} = 0.7$, $\gamma = 1.4$, $x = 1$.
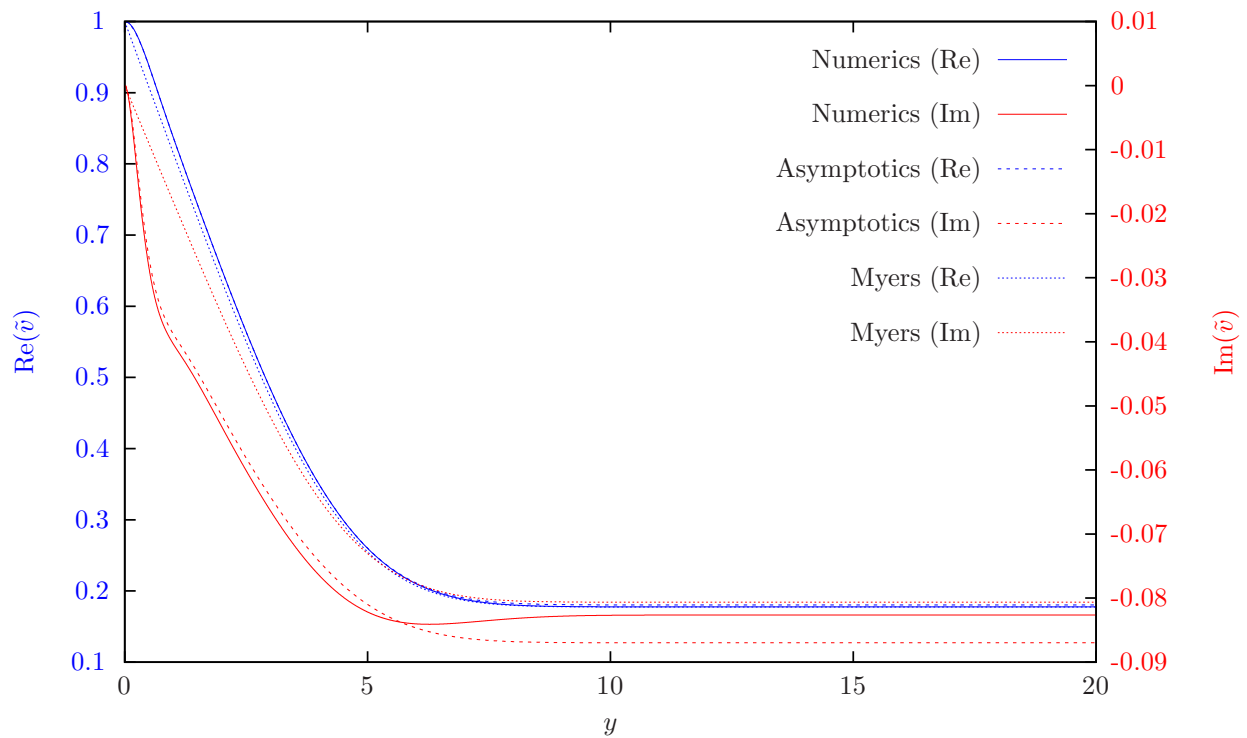

Figure 6. **Comparison of numerics and high-frequency asymptotics for** $\tilde{v}$ **for large** k **with** $\mathrm{Im}(k) > 0$. $k = 51 + 5\mathrm{i}$, $\omega = 31$, $M = 0.5$, $\mathrm{Pr} = 0.7$, $\gamma = 1.4$, $x = 1$.
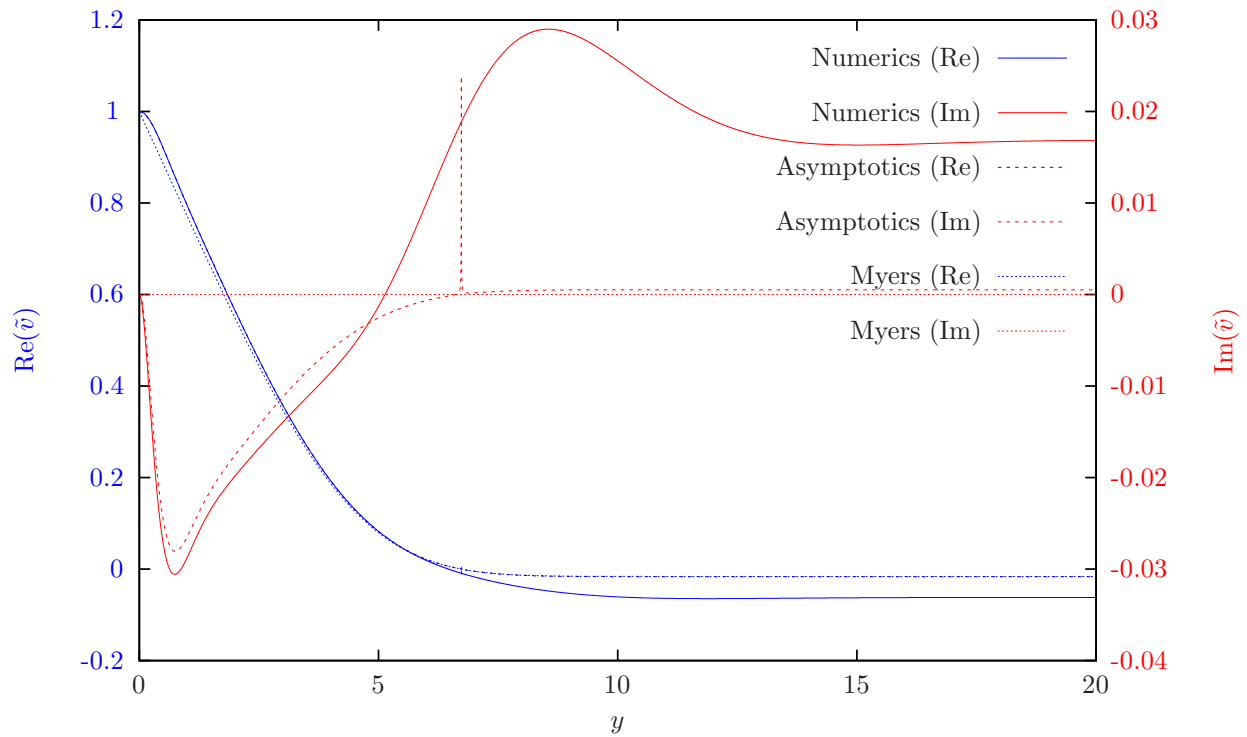
Figure 7. Comparison of numerics and high-frequency asymptotics for $\tilde{v}$ for large k with $\mathrm{Im}(k) = 0$; note the presence of a caustic, or critical layer. $k = 63$, $\omega = 31$, $M = 0.5$, $\mathrm{Pr} = 0.7$, $\gamma = 1.4$, $x = 1$.
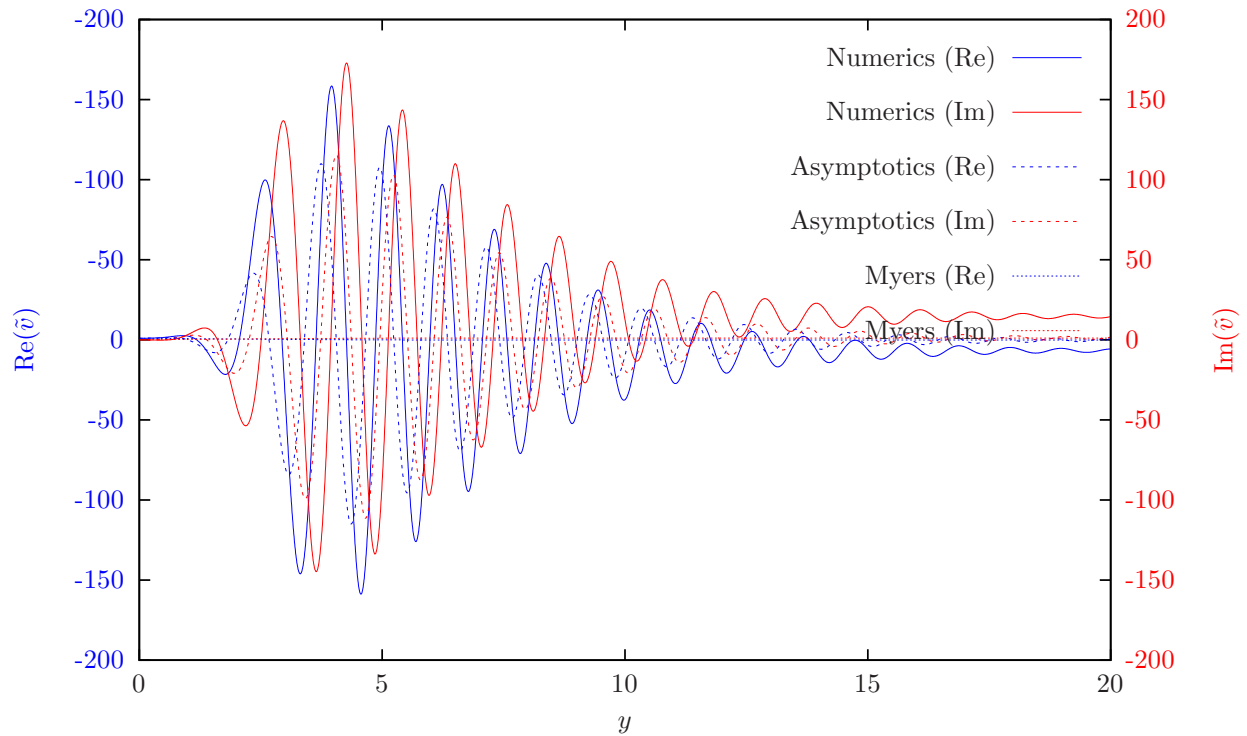

Figure 8. Comparison of numerics and high-frequency asymptotics for $\tilde{v}$ for large k with $\mathrm{Im}(k) < 0$; note the large scales on the y-axes. $k = 70 - 70i$, $\omega = 31$, $M = 0.5$, $\mathrm{Pr} = 0.7$, $\gamma = 1.4$, $x = 1$.
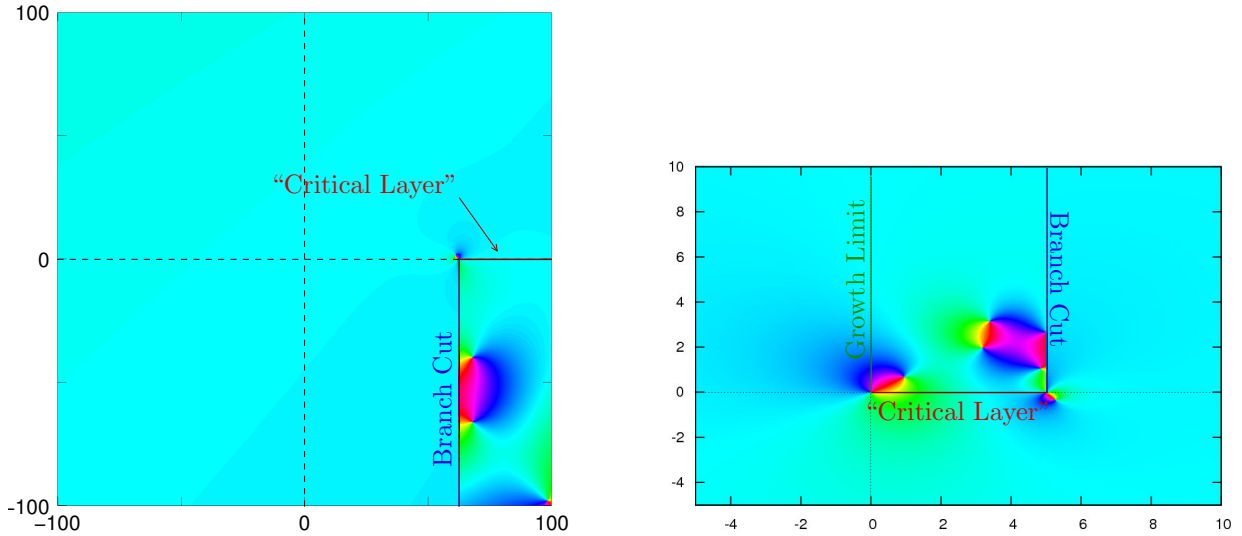
Figure 9. Sketch of high-frequency asymptotic region boundaries in the k-plane (left, $\omega = 31$) and the ω-plane (right, $k = 10$), together with $\arg(Z_{\text{eff}}/Z_{\text{disp}})$ (colour background). $M = 0.5$, $\text{Pr} = 0.7$, $\gamma = 1.4$, $x = 1$.

C.   Comparison of numerics and low-frequency asymptotics

Figure 10 plots the argument of $Z_{\text{eff}}/Z_{\text{mass}}$, for $k = 0.1$. The colours and the scale are the same as the right hand plot in figure 3. About the origin, the colour indicates that $Z_{\text{eff}}/Z_{\text{mass}}$ is real, and indeed looking at the raw data shows that $Z_{\text{eff}}/Z_{\text{mass}} \to 1$ as $\omega \to 0$. This verifies the low-frequency predictions of Ref. 23 and the low-frequency asymptotics of §V.A. Note, for comparison, that $Z_{\text{eff}}/Z_{\text{disp}}$ has a pole at $\omega = 0$.

VII.   Conclusion

In this paper, we have considered the effect of a laminar parallel viscous compressible boundary layer on the impedance of a fixed permeable boundary. This follows on from the work of Aurégan, Starobinski & Pagneux,[23] extending their asymptotics to allow for non-small Mach numbers, and from the numerous works using the Pridmore-Brown equation[22] to investigate the effect of sheared mean flow in ducts.[19–21] All such works have assumed, as we have here, that the mean flow is laminar and parallel.

The main result of this paper is the discovery of a region of the k- and ω-planes in the high-frequency limit where the Myers boundary condition does not hold. This region was not discovered previously, since it requires both dissipative terms (which are neglected for Pridmore-Brown analyses) and $|k| > |\omega/M|$, the latter never being true in the low Mach number limit considered in Ref. 23. One of the boundaries of this region is connected to the critical layer of the Pridmore-Brown equation, where the convective term vanishes (so for $y = y_0$ where $\omega - u(y_0)k = 0$). While the dissipative terms were shown in §IV.F to regularize the exact solution across this critical layer, it still persists as a caustic in the high-frequency multiple scales asymptotics. Another important boundary is the branch cut, which corresponds to undamped viscous waves outside the boundary layer.

For all the examples given here, the boundary-layer flow profile used is a compressible Blasius boundary layer (as shown in figure 2). However, the flow profile could be arbitrary, and the mathematics above would hold true for any laminar parallel flow profile. One of the new results of this paper is the first order correction to the Myers boundary condition in the high-frequency limit, given in (12). This correction term depends only on the derivative of the mean-flow velocity profile at the boundary, $u_y(0)$, and is otherwise independent of the boundary-layer flow profile.

The parallel flow assumption was justified here by considering a Blasius boundary layer far downstream of the leading edge generating it, so that $x \gg 1$; despite this, boundary layer thicknesses related to $x = 1$ have been used throughout for numerical examples, as this relates well to the flow in an aeroengine intake one
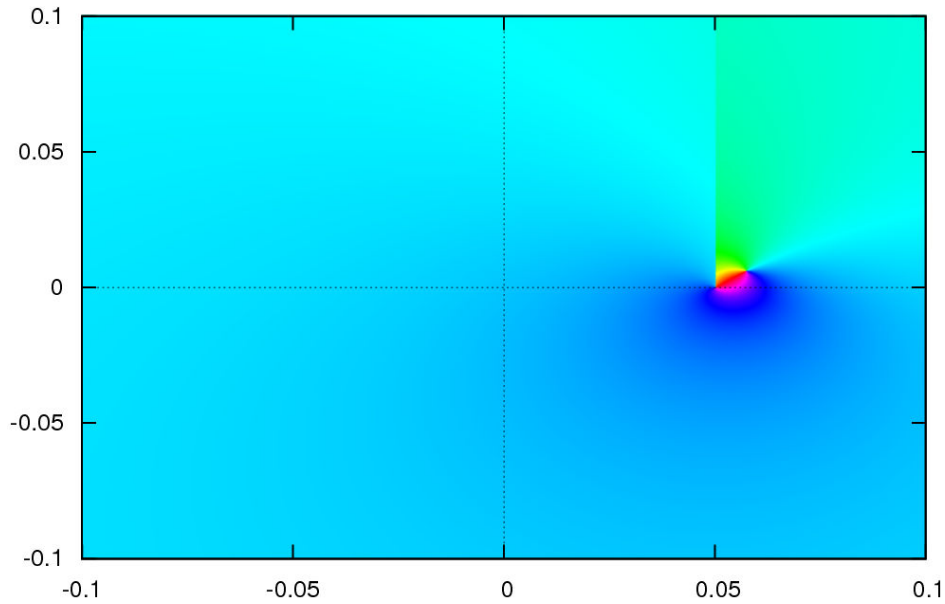
Figure 10. Plot of $\arg(Z_{\text{eff}}/Z_{\text{mass}})$ **in the** ω**-plane:** $k = 0.1$, $M = 0.5$, $\text{Pr} = 0.7$, $\gamma = 1.4$, $x = 1$.

duct radius downstream of the intake lip. The validity of the parallel assumption in this case is questionable. The parallel assumption could be expected to be far more realistic for well-developed flow, such as in ducts used for ground-based testing of acoustic linings,[24] for which $x \simeq 100$.

The laminar flow assumption is mainly related to the difficulty (or impossibility) of modeling acoustics across a turbulent boundary layer. The boundary layer in ground-based acoustic lining experiments is usually well-developed and turbulent,[24] though the nature of the boundary layer in aeroengine intakes is a more difficult question.

It is interesting to note that the validity of these assumptions differs between ground-based acoustic lining experiments, such as Ref. 24, and aeroengine intakes in flight. The different parameters and assumptions in these two cases are contrasted in table 3.

	In Flight	Ground Test
Mach number	≈ 0.5	$0 - 0.4$
Reynolds number (based on c_0)	$\approx 3 \times 10^7$	6×10^5
Prandtl number	0.7	0.7
Frequency (ω)	$2 - 200$	$0.2 - 1.6$
BL Thickness ($\sqrt{x}$)	≈ 1 ?	≈ 10
BL Type	?	turbulent
Duct cross-section	cylindrical	rectangular

Table 3. Comparison of nondimensional parameters and modelling assumptions between an aeroengine intake in flight and a ground-based acoustic lining test (such as Ref. 24).

One major outstanding question from this paper is, when solving for duct modes using the boundary impedance Z_{eff} calculated from (5), what is the behaviour of $\omega(k)$ for real k? The problem of instability for numerically modelling sound in acoustically-lined ducts with flow[9–14] is caused by $\text{Im}(\omega(k))$ being unbounded below for real k.[8] It is currently unclear whether the presence of a viscous boundary layer prevents this unbounded behaviour, and work is ongoing on this.

American Institute of Aeronautics and Astronautics Paper 2009-3241

References

[1]Eversman, W. and Beckemeyer, R. J., "Transmission of Sound in Ducts with Thin Shear Layers — Convergence to the Uniform Flow Case," *J. Acoust. Soc. Am.*, Vol. 52, 1972, pp. 216–220.

[2]Tester, B. J., "Some Aspects of "Sound" Attenuation in Lined Ducts containing Inviscid Mean Flows with Boundary Layers," *J. Sound Vib.*, Vol. 28, 1973, pp. 217–245.

[3]Myers, M. K., "On the Acoustic Boundary Condition in the Presence of Flow," *J. Sound Vib.*, Vol. 71, 1980, pp. 429–434.

[4]Tam, C. K. W. and Auriault, L., "Time-Domain Impedance Boundary Conditions for Computational Aeroacoustics," *AIAA J.*, Vol. 34, No. 5, 1996, pp. 917–923.

[5]Astley, R. J., Hii, V., and Gabard, G., "A Computational Mode Matching Approach for Propagation in Three-Dimensional Ducts with Flow," AIAA paper 2006-2528, 2006.

[6]Brambley, E. J. and Peake, N., "Surface-Waves, Stability, and Scattering for a Lined Duct with Flow," AIAA paper 2006-2688, 2006.

[7]Rienstra, S. W., "Acoustic Scattering at a Hard–Soft Lining Transition in a Flow Duct," *J. Engng Maths*, Vol. 59, 2007, pp. 451–475.

[8]Brambley, E. J., "Fundamental Problems with the Model of Uniform Flow over Acoustic Linings," *J. Sound Vib.*, Vol. 322, 2009, pp. 1026–103.

[9]Richter, C. and Thiele, F. H., "The Stability of Time Explicit Impedance Models," AIAA paper 2007-3538, 2007.

[10]Özyörük, Y., Long, L. N., and Jones, M. G., "Time-Domain Numerical Simulation of a Flow–Impedance Tube," *J. Comput. Phys.*, Vol. 146, 1998, pp. 29–57.

[11]Chevaugeon, N., Remacle, J.-F., and Gallez, X., "Discontinuous Galerkin Implementation of the Extended Helmholtz Resonator Model in Time Domain," AIAA paper 2006-2569, 2006.

[12]Richter, C., Thiele, F. H., Li, X., and Zhuang, M., "Comparison of Time-Domain Impedance Boundary Conditions for Lined Duct Flows," *AIAA J.*, Vol. 45, No. 6, 2007, pp. 1333–1345.

[13]Busse, S., Richter, C., Thiele, F. H., Heuwinkel, C., Enghardt, L., Röhle, I., Michel, U., Ferrante, P., and Scofano, A., "Impedance Deduction Based on Insertion Loss Measurements of Liners under Grazing Flow Conditions," AIAA paper 2008-3014, 2008.

[14]Tam, C. K. W., Ju, H., and Chien, E. W., "Scattering of Acoustic Duct Modes by Axial Liner Splices," *J. Sound Vib.*, Vol. 310, 2008, pp. 1014–1035.

[15]Nilsson, B. and Brander, O., "The Propagation of Sound in Cylindrical Ducts with Mean Flow and Bulk-reacting Lining: I. Modes in an Infinite Duct," *J. Inst. Maths Applics*, Vol. 26, 1980, pp. 269–298.

[16]Koch, W. and Möhring, W., "Eigensolutions for Liners in Uniform Mean Flow Ducts," *AIAA J.*, Vol. 21, No. 2, 1983, pp. 200–21.

[17]Rienstra, S. W., "A Classification of Duct Modes based on Surface Waves," *Wave Motion*, Vol. 37, 2003, pp. 119–135.

[18]Özyörük, Y., Alpman, E., Ahuja, V., and Long, L. N., "Frequency-Domain Prediction of Turbofan Noise Radiation," *J. Sound Vib.*, Vol. 270, 2004, pp. 933–950.

[19]Brooks, C. J. and McAlpine, A., "Sound Transmission in Ducts with Sheared Mean Flow," AIAA paper 2007-3545, 2007.

[20]Vilenski, G. G. and Rienstra, S. W., "On Hydrodynamic and Acoustic Modes in a Ducted Shear Flow with Wall Lining," *J. Fluid Mech.*, Vol. 583, 2007, pp. 45–70.

[21]Vilenski, G. G. and Rienstra, S. W., "Numerical Study of Acoustic Modes in Ducted Shear Flow," *J. Sound Vib.*, Vol. 307, 2007, pp. 610–626.

[22]Pridmore-Brown, "Sound Propagation in a Fluid Flowing Through an Attenuating Duct," *J. Fluid Mech.*, Vol. 4, 1958, pp. 393–406.

[23]Aurégan, Y., Starobinski, R., and Pagneux, V., "Influence of Grazing Flow and Dissipation Effects on the Acoustic Boundary Conditions at a Lined Wall," *J. Acoust. Soc. Am.*, Vol. 109, 2001, pp. 59–64.

[24]Jones, M. G., Watson, W. R., and Parrott, T. L., "Benchmark Data for Evaluation of Aeroacoustic Propagation Codes with Grazing Flow," AIAA paper 2005-2853, 2005.

[25]Burak, M. O., Billson, M., Eriksson, L.-E., and Baralon, S., "Validation of a Time & Frequency Domain Grazing Flow Acoustic Liner Model," AIAA paper 2008-2929, 2008.

[26]Prangsma, G. J., Alberga, A. H., and Beenakker, J. J. M., "Ultrasonic Determination of the Volume Viscosity of N_2, CO, CH_4 and CD_4 between 77 and 300K," *Physica*, Vol. 64, 1973, pp. 278–288.

[27]Landau, L. D. and Lifshitz, E. M., *Fluid Mechanics*, Elsevier, 2nd ed., 1987.

[28]Schlichting, H., *Boundary-layer Theory*, McGraw-Hill, 3rd ed., 1968.

[29]Rienstra, S. W., "Sound Transmission in Slowly Varying Circular and Annular Lined Ducts with Flow," *J. Fluid Mech.*, Vol. 380, 1999, pp. 279–296.

[30]Goldstein, M. E., "Unsteady Vortical and Entropic Distortions of Potential Flows Round Arbitrary Obstacles," *J. Fluid Mech.*, Vol. 89, 1978, pp. 433–468.

[31]Anderson, E., Bai, Z., Bischof, C., Blackford, S., Demmel, J., Dongarra, J., Du Croz, J., Greenbaum, A., Hammarling, S., McKenney, A., and Sorensen, D., *LAPACK Users' Guide*, Society for Industrial and Applied Mathematics, 1999.

[32]Brambley, E. J. and Peake, N., "Classification of Aeroacoustically Relevant Surface Modes in Cylindrical Lined Ducts," *Wave Motion*, Vol. 43, 2006, pp. 301–310.